RESEARCH ARTICLE

3D printing of PCL-ceramic composite scaffolds for bone tissue engineering applications

Santosh Kumar Parupelli^{1,3}, Sheikh Saudi², Narayan Bhattarai^{2,3}, and Salil Desai^{1,3}*

¹Department of Industrial and Systems Engineering, North Carolina A&T State University, Greensboro, NC 27411, USA

²Department of Chemical, Biological and Bioengineering, North Carolina A&T State University, Greensboro, NC 27411, USA

³Center of Excellence in Product Design and Advanced Manufacturing, North Carolina A&T State University, Greensboro, NC 27411, USA

(This article belongs to the Special Issue: Additive Manufacturing of Functional Biomaterials)

Abstract

Three-dimensional (3D) printing was utilized for the fabrication of a composite scaffold of poly(ε-caprolactone) (PCL) and calcium magnesium phosphate (CMP) bioceramics for bone tissue engineering application. Four groups of scaffolds, that is, PMC-0, PMC-5, PMC-10, and PMC-15, were fabricated using a custom 3D printer. Rheology analysis, surface morphology, and wettability of the scaffolds were characterized. The PMC-0 scaffolds displayed a smoother surface texture and an increase in the ceramic content of the composite scaffolds exhibited a rougher structure. The hydrophilicity of the composite scaffold was significantly enhanced compared to the control PMC-0. The effect of ceramic content on the bioactivity of fibroblast NIH/3T3 cells in the composite scaffold was investigated. Cell viability and toxicity studies were evaluated by comparing results from lactate dehydrogenase (LDH) and Alamar Blue (AB) colorimetric assays, respectively. The live-dead cell assay illustrated the biocompatibility of the tested samples with more than 100% of live cells on day 3 compared to the control one. The LDH release indicated that the composite scaffolds improved cell attachment and proliferation. In this research, the fabrication of a customized composite 3D scaffold not only mimics the rough textured architecture, porosity, and chemical composition of natural bone tissue matrices but also serves as a source for soluble ions of calcium and magnesium that are favorable for bone cells to grow. These 3D-printed scaffolds thus provide a desirable microenvironment to facilitate biomineralization and could be a new effective approach for preparing constructs suitable for bone tissue engineering.

Keywords: 3D printing; Bio-ceramics; Composites; Bone; Scaffold; Tissue engineering

*Corresponding author: Salil Desai (sdesai@ncat.edu)

Citation: Parupelli SK, Saudi S, Bhattarai N, *et al.* 2023, 3D printing of PCL-ceramic composite scaffolds for bone tissue engineering applications. *Int J Bioprint.*

https://doi.org/10.36922/ijb.0196

Received: September 11, 2022 Accepted: November 18, 2022 Published Online: July 5, 2023

Copyright: © 2023 Author(s). This is an Open Access article distributed under the terms of the Creative Commons Attribution License, permitting distribution, and reproduction in any medium, provided the original work is properly cited.

Publisher's Note: AccScience Publishing remains neutral with regard to jurisdictional claims in published maps and institutional affiliations.

1. Introduction

Tissue engineering (TE) is an interdisciplinary field that emerged as a promising technique that utilizes cells, biomaterials, biochemical (e.g., growth factors), and physical (e.g., mechanical loading) signals to generate new tissue structures. The goal of TE is to improve, replace, or restore damaged tissues or organs from any causes, such as disease,

defect, trauma, or aging. TE aims to create functional organs from patients' cells. The process of TE starts with biomaterials, followed by the fabrication of scaffolds, combining them with cells and biochemical signals, such as growth factors, cytokines, mechanical stimulants, to generate new tissue structures^[1,2]. Microfabrication techniques used in TE include photolithography, rapid prototyping (stereolithography, extrusion deposition printing), and soft lithography (microcontact printing, micro-molding, and microfluidics)[2]. "A biomaterial is a substance that has been engineered to take a form which, alone or as part of a complex system, is used to direct, by control of interactions with components of living systems, the course of any therapeutic or diagnostic procedure, in human or veterinary medicine" [3-6]. Biomaterials are derived from several sources such as natural materials, synthetic polymers, metals, ceramics, and composites^[7,8]. Naturally derived biomaterials include protein-based biomaterials (silk fibroin, keratin, collagen, gelatin, fibrin, and eggshell membrane) and polysaccharide-based biomaterials (chondroitin, glucose, cellulose, alginate, hyaluronan, and chitin and its derivative chitosan), and decellularized tissue biomaterials. Synthetic polymers for tissue regeneration include polylactic acid (PLA), polyglycolic acid (PGA), poly (lactic-co-glycolic acid) (PLGA), and polyurethanes. Metals include titanium alloys, nitinol, magnesium alloys, stainless steel, and cobalt-chromium alloys. Composites include metal-ceramic, metal-polymer, and polymer-ceramic^[9-11]. Each of the above-mentioned individual biomaterial groups has specific advantages and disadvantages. Biomaterials have played a crucial role in supporting and fostering regenerative cell growth in the tissue engineering design paradigm and biomedical devices for numerous clinical regenerative therapies^[12-18].

Scaffolds are temporary structures that mimic physical microstructures of a natural extracellular matrix (ECM) to provide desired cellular interactions and guide cells to grow, synthesize, and other biological molecules to form new functional tissues [2]. To engineer functional tissues and organs successfully, scaffolds should possess the minimum requirements, such as high porosity, proper degradation rate, biocompatible, high surface area, mechanical integrity, enhanced cell adhesion, growth, differentiated function, and migration^[19]. Cell proliferation, attachment, and differentiation are affected strongly by the scaffold microenvironment, including the size, density of the pores, geometry, surface properties, and windows connecting the pores^[20]. Techniques include porogen leaching, phase separation, uniaxial freezing, micro-molding, gas foaming, fiber meshes/fiber bonding, electrospinning, and additive manufacturing (laser-based, nozzle-based, and printer-based) are used for the fabrication of scaffolds^[21-23].

fundamental concepts that lead to establishment of bone tissue-engineered scaffolds are typically based on the selected biomaterial and production technique. Generally, for bone TE, pore sizes between 100 and 350 micrometers and porosities more than 90% are preferred. PCL is a biodegradable polymer like other degradable hydroxy polyesters such as PGA, poly-llactic acid (PLLA), and their copolymers. PCL is one of the widely studied synthetic polymers in different formulations for TE due to its elastomeric mechanical properties and biological properties. PCL is a rigid, flexible polymer with a semi-crystalline structure having high thermal stability, low glass transition (-60°C), and melting temperatures (56-65°C). The slower degradation rate and mechanical properties limit the use of PCL compared to other polyester family members. However, the degradation kinetics and mechanical strength of the PCL can be tailored by copolymerization or blending with other polyesters or ceramic materials. PCL can be used for scaffold fabrication for bone, liver, cartilage, skin, and protein delivery vehicles^[24-28].

Numerous studies have been done on the blending of PCL with several bioceramics (e.g., calcium phosphate, magnesium phosphate, biphasic calcium phosphate, hydroxyapatite, and bioactive glass), natural polymers (chitosan, elastin, collagen, gelatin, and silk), and synthetic polymers (PLGA, PGA, PLLA, and carbon nanotubes) to enhance the mechanical endurance and biocompatibility of the scaffolds^[29]. Magnesium phosphate/PCL (MP/PCL) composite scaffold enhances the polymer's degradation rate by improving the PCL hydrophilicity^[30,31]. Moreover, the surface wettability of the MP/PCL can be tailored by adjusting the amount of MP particles incorporated[32]. Blending nano-hydroxyapatite (nHA) with PCL improves composite polymer scaffold strength (mechanical property) and bioactivity[33]. Biocomposite scaffolds made from polycaprolactone (PCL) and forsterite bioceramics can enhance and modulate mechanical and physical properties^[34,35]. Incorporating aluminum oxide whiskers within PCL significantly improves the composite scaffold's mechanical and hydrophilic surface properties with good biocompatibility for TE and dental applications^[36]. Composite scaffolds prepared with calcium alginate threads and PCL demonstrate ideal porosity grade with suitable microstructure for enhanced bone cell growth and differentiation^[25]. The presence of β-tricalcium phosphate (TCP) in PCL improves the cell proliferation and compressive mechanical properties of the composite scaffold for bone regeneration[31,37-41].

Magnesium phosphate and calcium phosphate-based bioceramics are well-known in the biomaterials field and have been used separately with PCL scaffolds. However, the calcium magnesium phosphate (CMP) bio-ceramics, a combined phosphate of magnesium and calcium, have not been thoroughly studied. Therefore, our strategy in this study is to first develop an optimal composition of CMP bioceramic powder. Our second strategy is to develop a slurry of ceramic powder and PCL in a good organic solvent that is suitable for three-dimensional (3D) printing. Third, we optimize the properties of the 3D-printed scaffolds so that the methodology and knowledge gained from this research will be applied for bone TE applications in the future.

Additive manufacturing (AM) techniques enable the fabrication of complex geometry scaffolds for TE applications^[42-44]. 3D bioprinting enables the fabrication of tissue or organs using biomaterials and cells in a layerby-layer fashion from the bottom up using computeraided design (CAD) model data^[45]. The three main fundamental approaches 3D bioprinting is based on are as follows: (i) biomimicry, (ii) autonomous selfassembly, and (c) mini tissue building blocks. Different types of AM techniques that can be used for bioprinting include extrusion-based printing, inkjet-assisted printing, and droplet-based printing[46,47]. The extrusion 3D printing process is the most popular technique. With 3D bioprinting, complex tissue structures that mimic the fine shape and size of the targeted natural original tissue can be fabricated with personalized features. The applicability of 3D bioprinting to biomedical devices, pharmaceutics, and regenerative medicine has increased as a result of recent breakthroughs in reinforcement strategies, hydrogel chemistries, and crosslinking techniques^[48]. Biocompatibility of the material being used, growth factor distribution, perfusion, and cell sensitivity to the printing procedures are some of the crucial aspects of bioprinting, that must be taken into consideration because 3D bioprinting works with living organisms such as cells and tissues^[49]. In the past decade, numerous research studies have been reported on optimizing AM techniques for 3D scaffold fabrication with desired mechanical and biological properties for cell growth in regenerative medicine^[50-55]. In this research, we utilized the direct-write AM technique to fabricate a composite scaffold with CMP bio-ceramic and PCL materials for bone TE application. In our experiments, four groups of scaffolds - PMC-0: PCL (50% w/v), PMC-5: PCL (50% w/v)/CMP(5%w/w), PMC-10: PCL (50% w/v)/CMP (10%w/w), and PMC-15: PCL (50% w/v)/CMP (15%w/w) - were fabricated using a custom-built 3D printer. The effect of ceramic content on the surface properties, biodegradability, and bioactivity of fibroblast cells on the composite scaffold was investigated. A customized functionally gradient scaffold structure was fabricated to demonstrate that manipulation of surface and biological properties can be achieved for the enhanced spatial organization of cells within the composite scaffold.

2. Materials and methods

Poly(ε-caprolactone) pellets (PCL, Mw = 43,000 g/mol) with a melting point of 58 – 64°C were purchased from Polysciences Inc. (Warrington, PA, USA). 2,2,2-Trifluoroethanol (TFE) was purchased from Sigma-Aldrich (St. Louis, Mo, USA). Magnesium oxide (MgO) nanopowder (size < 50 nm) and calcium phosphate monobasic were purchased from Sigma Aldrich (St. Louis, MO, USA). Dulbecco's modified Eagle's medium (DMEM) was purchased from Life Technologies (Grand Island, NY, USA). The Alamar Blue and lactate dehydrogenase (LDH) assay kits were purchased from Thermo-scientific (Waltham, MA or Florence, KY).

2.1. Synthesis of CMP bioceramics

CMP ceramic was prepared using a mixture of MgO and calcium phosphate monobasic according to a previously published paper^[56]. MgO was first dissolved in water, and calcium phosphate was added with a 2:1 molar ratio (3.2:1 w/w). The mixture was vortexed for 5 min and then poured into a Petri dish. The Petri dish was kept in a fume hood for 24 h to dry up all water from the mixer. Fine powder of the CMP was stored in a desiccator. Four concentrations of the polymer and ceramic material in different proportions were formulated for the subsequent experiments.

2.2. Production of PCL/CMP suspension

Initially, 50% (w/v) PCL was prepared by suspending 5 g of PCL pellets in 10 mL of TFE and ultra-sonicated at 45°C for 2 h to produce PCL-only scaffolds. To produce PCL-CMP composite scaffolds, the predetermined content of the CMP (5, 10, and 15 wt % in relation to the PCL polymer) was dispensed into 10 mL of TFE through ultrasonication at 45°C for 2 h. The experimental procedure to produce PCL-CMP suspension is illustrated in Figure 1.

Pellets of PCL (5 g) were added to the TFE solvent containing the CMP and then mixed using magnetic stirring for 24 h. Similarly, PCL-CMP composites with a CMP content of 10% and 15% were also prepared. Each composition of the suspension is shown in Table 1. A 100-mm filter was used to filter all the CMP solutions to avoid clogging during printing.

2.3. 3D printing of scaffolds

A four-axis Nordson EFD Janome robot with a custom extrusion head, as shown in Figure 2, was used to fabricate 3D scaffold structures. All material concentrations were loaded into a 10 mL syringe barrel with a nozzle of 250 μm

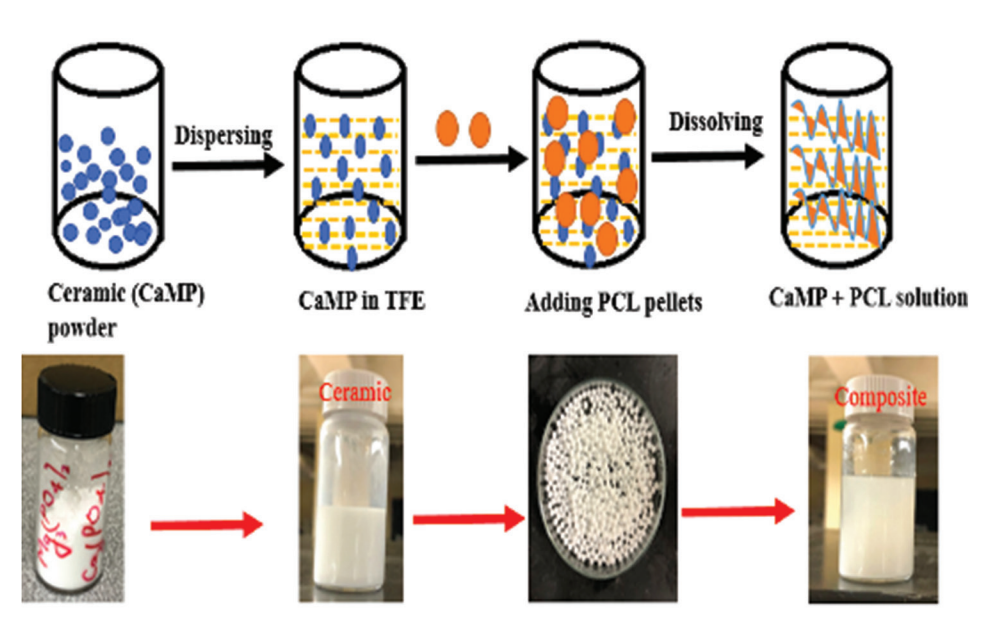


Figure 1. Experimental procedure to produce PCL-CMP suspension.

Table 1. Suspension sample compositions

Composite scaffolds	CMP (g)	TFE (ml)	PCL (g)	CMP (w/w%) in the scaffold
PMC-0	0	10	5	0
PMC-5	0.25	10	5	5
PMC-10	0.5	10	5	10
PMC-15	1.0	10	5	15

diameter. The syringe barrel consisting of the PCL/CMP suspension was attached with a piston and connected to a pressure system (Ultimus V) to alter the flow rate. A cuboidal 3D scaffold structure ($10 \times 10 \times 0.2$ mm) was generated in CAD, and exported as a stereolithography (STL) file, and the x, y, and z coordinates of the STL file were imported into the robot with JRC 3D printing software. The PMCs struts were built layer-by-layer (12 layers: 0.2 mm) to build a 3D scaffold structure with uniform pore size and porosity. The struts were 0.2 mm in height, 10 mm in length, and 10 mm in width. All the process parameters, including line speed, extrusion pressure, nozzle diameter, spacing between the struts, and layer thickness, were kept consistent for all material concentrations.

2.4. Characterization of scaffolds

2.4.1. Rheology analysis

The rheological properties of all the material concentrations (PMCs) were measured using Rehocal DVIII T Rheometer. The shear stress of each material was measured at different shear rates (0-120/s) using an SC4 spindle at room temperature. The shear rate versus shear stress curves

for each material concentration was plotted using the Rheocalc T software.

2.4.2. Contact angle measurements

The surface wettability (hydrophilicity/hydrophobicity) of the PMC-0 and ceramic composite PMCs was tested using a Drop Shape analyzer (KRUSS-DSA25E) with the sessile drop method at room temperature. For all material concentrations, thin film samples were made and placed in Petri dishes. Five samples for each material concentration at 90 s were tested to calculate the average water contact angle. The sessile drop size was set to $5\,\mu L$.

2.4.3. Surface morphology analysis

The surface morphology of the ceramic powder was analyzed using a scanning electron microscope (SEM; Zeiss Auriga FIB/FESEM, Carl Zeiss Microscopy, LLC, NY, USA). Briefly, ceramic powder (0.1 g of as-prepared) was dispersed in 10 mL of TFE. A single drop of the ceramic suspension was deposited on an aluminum foil and attached to double-sided carbon tape. SEM (Zeiss Auriga FIB FE-SEM) images of printed samples and the CMP powder were taken at an accelerating voltage of 5 kV. Before SEM analysis, a thin layer of gold sputtering (10 nm) was applied to the samples. The effect of ceramic particles on the PCL matrix was investigated.

ImageJ open-source software^[57] was used to calculate the porosity of the scaffold. Color thresholds were varied to capture the boundaries of the pores using an edge detection algorithm. All pore dimensions were recorded with their sizes and respective pore areas. Image correction was

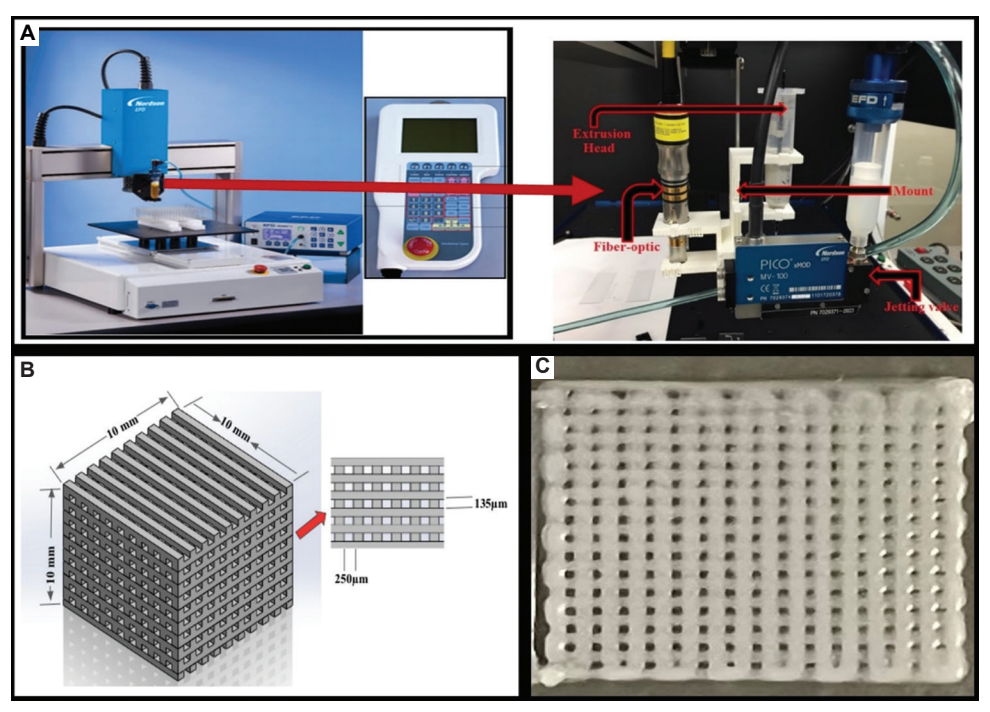


Figure 2. (A) Direct-write 3D printing custom equipment for scaffold fabrication. (B) 3D computer-aided design model of the ceramic composite scaffold. (C) 3D-printed composite ceramic scaffold.

performed to eliminate extraneous pores and provide the porosity of the scaffold. Porosity analysis was performed on a sample of three (n = 3).

2.4.4. X-ray diffraction (XRD)

The crystallography and phases of CMP were examined using a Bruker AXS D8 Discover X-ray diffractometer with Cu-K radiation. The XRD studies were carried out with a locked-coupled scan with a scanning range (diffraction angle, 2θ) of 15° – 60° . The instrument was run in continuous mode, with increments of 0.0146° for 2 min. An experiment was carried out at room temperature.

2.4.5. FT-IR analysis

Fourier-transform infrared spectroscopy (FT-IR) was used to identify the functional groups and chemical interactions between PCL and CMP. Varian 670 FT-IR Spectrophotometer (Varian, Inc., Palo Alto, CA, USA) was used to detect the spectra in the range of 4000 – 400 cm⁻¹ with 64 scans at a resolution of 4 cm⁻¹. A total of 5 scans were performed for each spectrum.

2.4.6. Biocompatibility study

The procedure to conduct biocompatibility was implemented based on our previous work^[29]. The 3D scaffold samples (n = 3) were cut (1 cm × 1 cm), glued with Surgical Silicone Adhesive, Kwik-SilTM, and attached to 24-well plates. Samples were sterilized with 95% ethanol

in a sterile fume hood for 30 min, followed by rinsing with sterile deionized water (twice) and 1× Dulbecco's phosphate-buffered saline (DPBS). Before cell seeding, 1 mL of DMEM supplemented with 10% fetal bovine serum (FBS) and 1% antibiotics (10,000 units/mL of penicillin and 10,000 µg/mL of streptomycin) was added to each well plate, which was placed in cell culture incubator for 3 h. NIH/3T3 cells, a mouse fibroblast cell line (American Tissue Type Culture Collection, Manassas, VA), were cultured in a 75 cm² culture flask and kept in a tissue culture incubator at 37°C and a 5% CO₂ atmosphere. Every 2 days, the culture medium was changed. The cells were separated by 0.025% trypsin and 0.01% EDTA in a phosphate-buffered saline (PBS) solution once they had reached around 90% confluence, followed by transferring them to a centrifuge tube with the culture medium. Before being seeded into samples, cells were resuspended in new growth media and counted with a hemocytometer using a CountessTM II Automated Cell Counter (Thermo Fisher Scientific). A 50 µL aliquot of medium containing cells (\sim 50,000) was placed on printed samples (n = 3) and cultured in an incubator (37°C, 5% CO₂) for 1, 2, and 3 days, respectively.

Alamar blue (AB) colorimetric assay was used to measure the viability of 3T3 cells after growth on substances. Cell culture medium was collected from each incubated sample and stored for toxicity study at a specific

time. After that, cells were washed 2 times with PBS and treated with 10% (v/v) AB reagent in the appropriate culture medium for 4 h. Multiple aliquots of the assay solutions were obtained and measured for fluorescence using a spectrophotometer with excitation at 530 nm and emission at 590 nm. The following equation was used to calculate the viability of cells:

$$Cell \ viability = \frac{- \ Fluorescence \ of \ the \ blank}{Fluorescence \ of \ the \ control} \times 100\%$$

$$- \ Fluorescence \ of \ the \ blank$$

LDH assay was carried out with the stored medium collected earlier.

2.4.7. Statistical analysis

Statistical analysis was performed using Minitab statistical software. Data are expressed as mean \pm standard deviation. Comparisons of groups were performed using one-way analysis of variance (ANOVA) and Tukey's *post hoc* test. Significance levels were set at P < 0.05.

3. Results and discussion

3.1. Rheology measurements

The rheological properties of the materials were studied to investigate the effect of CMP on the PCL matrix. The rheological measurements of the PCL and composite in terms of shear rate and shear stress are shown in Figure 3. All tests were performed in flow sweep mode across a range of shear rates from 0.1 to 120 s⁻¹. PMC-0, PMC-5, PMC-10, and PMC-15 exhibit a Newtonian region followed by

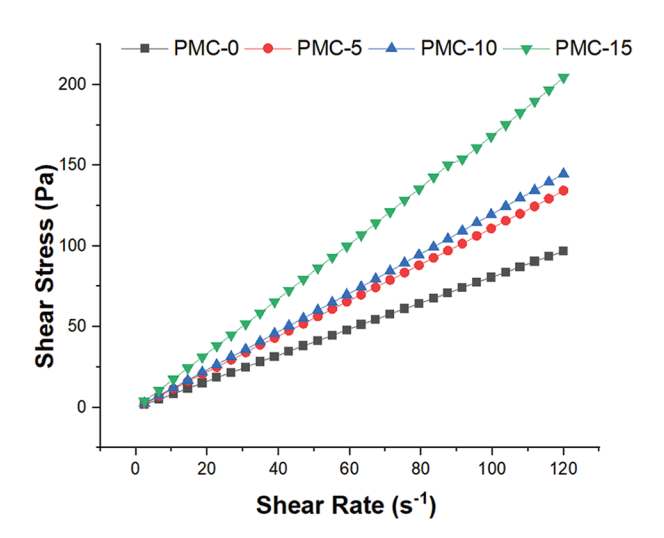


Figure 3. Rheology characteristics of PMCs suspensions. An increase in the microparticle content of ceramic material in the PCL matrix exhibit a non-Newtonian fluid behavior at higher shear rates.

non-Newtonian fluid behavior at higher shear rates. The non-Newtonian behavior represents a shear-thinning fluid as the shear rate increases beyond 80 s. The shear stress increased with an increase in the content of CMP, in the following order PMC-0 < PMC-5 < PMC-10 < PMC-15. With the addition of the CMP particles, the viscosity of the PMCs materials increased because of the interaction between the polymeric matrix (PCL) and the ceramic particles (CMP). The increase in the shear stress is due to the increase in the microparticle content of ceramic material in the polymer matrix, which leads to a higher resistance to the flow of fluid^[58,59]. Higher shear stress for increased PCL-CMP blends indicates an elasticity higher than that of pure PCL. The rheological behavior observed herein is vital as the bioprinter needs to be operated by varying parameters, such as deposition line speed, extrusion pressure, and nozzle size, to accommodate the shear-thinning behavior of the biomaterial being bioprinted. Moreover, higher extrusion pressures are needed to deposit higher PCL-CMP blends to maintain consistent scaffold geometries.

3.2. Characterization of ceramic powder

The as-prepared CMP ceramic was used for incorporation into the 3D-printed PCL scaffolds. SEM image (Figure 4) shows that the ceramic was a mixture of clay-like Ca₃(PO₄)₂ and spindle-shaped Mg₃(PO₄)₂ particles^[60]. About 2- – 5-micron (length) Mg₃(PO₄)₂ crystals were seen embedded into Ca₃(PO₄)₂ substances. The XRD pattern for CMP is shown in Figure 5 (left). XRD data for the particles, with peaks, are consistent with the known crystallographic planes of both phosphates. Mg₃(PO₄)₂ peaks are assigned by cross marks (x), and Ca₃(PO₄)₂ peaks are assigned by an asterisk (*) marks^[60]. Figure 5 (right) shows the FT-IR spectra of the ceramic powder. Absorption bands at 1060 cm⁻¹ and 970 cm⁻¹ were ascribed to PO₄³⁻, and

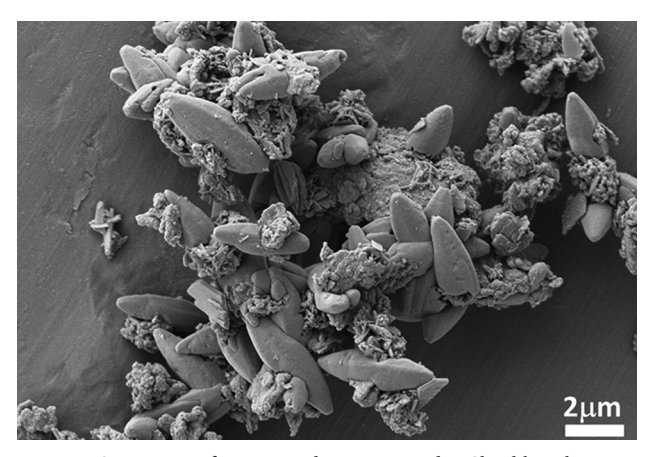


Figure 4. SEM image of as-prepared ceramic powder. Clay-like substances are $Ca_3(PO_4)_2$ and spindle-shaped substances are $Mg_3(PO_4)_2$.

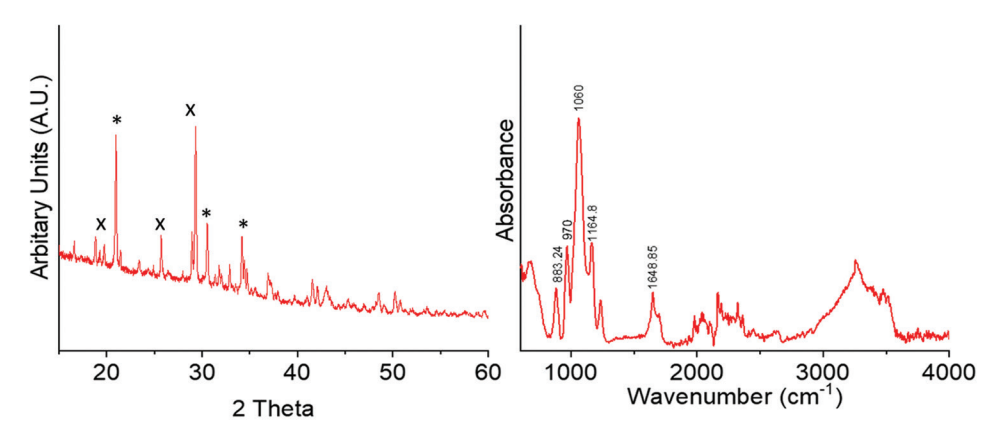


Figure 5. XRD pattern (left) and FT-IR spectra (right) of as-prepared CMP ceramic powder.

the band at 883.24 cm⁻¹ and 1164.8 cm⁻¹ correspond to the vibration of P–O–H from ${\rm Mg_3(PO_4)_2}$ and ${\rm Ca_3(PO_4)_2}$. Adsorbed water band is relatively wide, from 2600 cm⁻¹ to 3600 cm⁻¹ 9. The additional band at 1648.85 cm⁻¹ was observed due to H-O-H bending^[60]. These results indicate that the chemical composition of CMP bioceramics has both Ca and Mg phosphates.

3.3. Morphology analysis of 3D scaffolds

The morphology of the PCL and PCL-CMP composite scaffolds was investigated with an SEM. Figure 6 presents SEM micrographs of the top surface and cross-sectional morphology of the PMC-0, PMC-5, PMC-10, and PMC-15 scaffolds, respectively.

The SEM images illustrate that all the scaffolds exhibit well-defined structures with uniform pore size distribution. The pore size of the polymer and composite scaffolds was $200 \pm 35 \mu m$, marginally less than the designed scaffold (250 µm). The variations in the pore size are due to the rheological characteristics of materials. Typically, 3D printing processes provide precise dimensions and shapes of the features being printed. However, in this case, the PCL-ceramic composite materials (PMCs) were laden with solvent (TFE) to suit appropriate rheology for extrusion from the nozzle tip. Thus, after the deposition of these materials, there was a shrinkage after curing and evaporation of the water, leading to lower pore size as compared to the designed (250 µm) dimension. The PCL scaffolds appear to have a smooth surface compared to the PMC-5, PMC-10, and PMC-15. As the amount of ceramic content increased, the surface morphology of the composite scaffold exhibited a rough structure. The roughness of the composite scaffold surface is due to the dispersion of ceramic microparticles in the PCL matrix, which alters the morphology of PCL. This leads to a rougher surface with an increased surface area that closely mimics the natural ECM^[61,62]. The crucial characteristics that affect

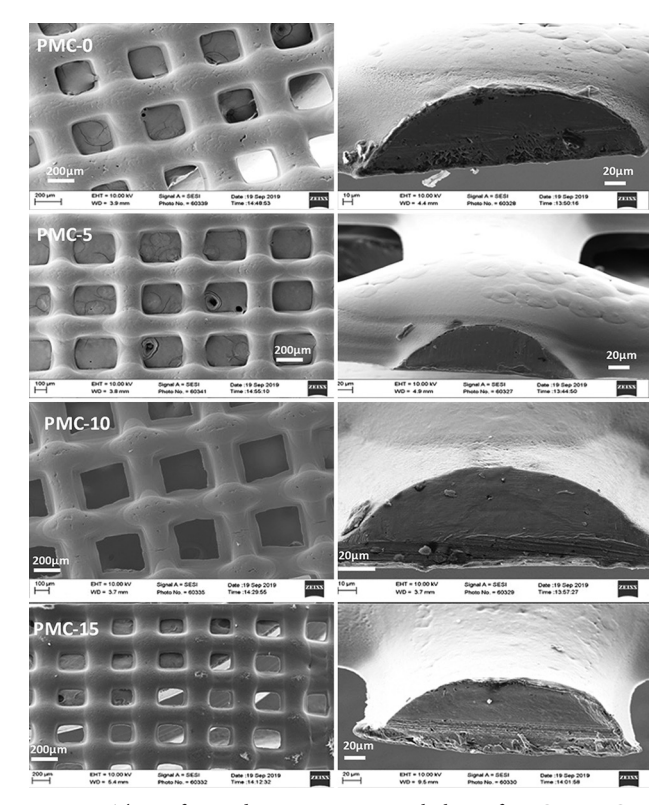


Figure 6. The surface and cross-section morphology of PMC-0, PMC-5, PMC-10, and PMC-15. Left: SEM images of 3D-printed scaffolds. Right: SEM images showing the cross-sectional view of the scaffold's single strut. The pore size of the composite scaffolds was in the range of $200 \pm 35 \ \mu m$.

cell adhesion and proliferation are porosity and surface roughness of the scaffold, as mentioned elsewhere^[63-65]. The rheological changes were tailored by adding ceramic microparticles, which altered the properties such as shear stress, viscosity, and interaction between flow material and nozzle wall. Hence, the PCL and composite scaffold surface characteristics reacted differently under similar process conditions.

3.4. Porosity of scaffolds

The pore size and porosity of the 3D-printed scaffolds were calculated and are presented in Table 2. The virgin polymer PMC-0 had the largest pore size (~245 μ m) and the highest porosity (50%), respectively. However, as the ceramic content within the scaffold increased, there was a reduction in both the pore size and porosity. This can be attributed to the increase in ceramic loading within the polymer composite that leads to higher viscosities of the 3D-printed slurries. This finding correlates well with the rheological behavior of the PMC suspension as shown in Figure 3, wherein higher microparticle loading has revealed a non-Newtonian behavior. However, it is noteworthy to point out that pore sizes above 150 μ m and porosities above 40% are conducive

Table 2. Comparative analysis of pore size and porosity for PMC scaffolds

Material composition	Pore size (µm)	Porosity (%)
PMC-0	245.5±20.5	50.61±0.34
PMC-5	234.3±22.4	48.32±0.23
PMC-10	222.8±23.2	45.54±0.71
PMC-15	213.4±18.7	42.34±0.56

for facilitating the diffusion of nutrition, allowing cell migration, accelerating cell proliferation, and enabling vascularization^[66-68]. Thus, our high-porosity scaffolds provide diffusion and release pathways of biological molecules and nutrients for cellular migration and proliferation^[69,70].

3.5. Hydrophilicity behavior of scaffolds

The surface wettability of the scaffolds, which affects cell proliferation and protein absorption, can be determined by the water contact angle. Hydrophilicity plays a crucial role in cell interaction within the scaffold. The hydrophilicity of the PMC-0, PMC-5, PMC-10, and PMC-15 was analyzed by measuring the incident contact angle at two different durations (initial at 3 s and equilibrium 90 s) using a drop shape analyzer (KRUSS-DSA25E) as shown in Figure 7.

Figure 8 shows the water contact angle measurements of polymer and composite scaffolds. The contact angle for our blend of PMC-0 was around $94.31 \pm 3.21^{\circ}$ as compared to pure PCL reported in the literature at $109.2 \pm 4.1^{\circ [71]}$. However, the PMC-5, PMC-10, and PMC-15 composites had consistently lower contact angles (PMC-5: $74.5 \pm 2.23^{\circ}$; PMC-10: $68.9 \pm 2.15^{\circ}$; and PMC-15: $67.8 \pm 2.03^{\circ}$). The incorporation of CMPs increased the hydrophilicity of

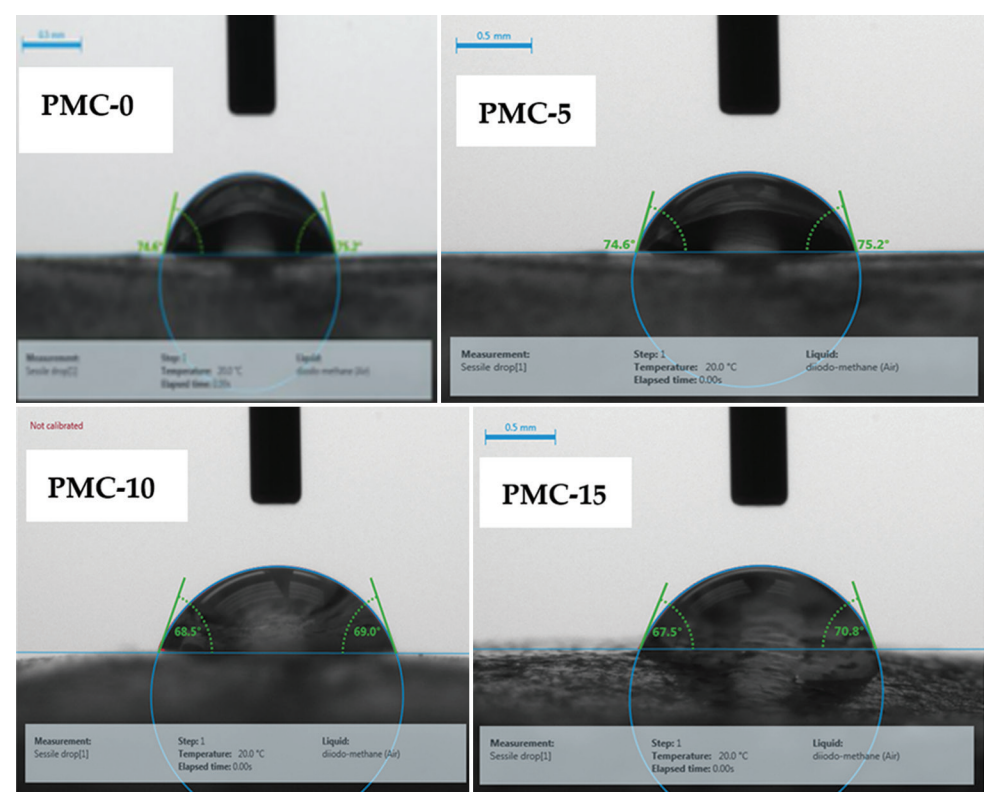


Figure 7. Water contact angle measurement of different contents of PMCs scaffolds.

the composite scaffolds. The decreasing order of contact angle measurements with an increase of bio-ceramics resembles well with decreasing trend as seen in PCL/HA composite scaffold structures^[59]. These results illustrate that homogeneously mixed PMCs resulted in an enhanced hydrophilic scaffold, which can further improve the cellular proliferation and adsorption of biochemical cues for orthopedic applications, as reported in our previous computational biochemical models^[31,55].

Moreover, researchers can tune the hydrophilicity and cellular response by adjusting the amount of CMPs in the scaffold structures. Furthermore, multi-nozzle deposition 3D bioprinting can provide functionally gradient PMCs structures for osteochondral (bone-cartilage) tissue constructs by manipulating material and process parameters. In the past, a variety of biological materials, including ECM, adhesion proteins, such as collagen, laminin, and fibronectin, as well as mucopolysaccharides, such as heparin sulfate, hyaluronate, and chondroitin sulfate, both individually and as mixtures have been applied to promote cell adhesion^[51,53]. The current synthetic hydrophilic polymeric coatings show an analogous improvement in the attachment and growth of cell lines.

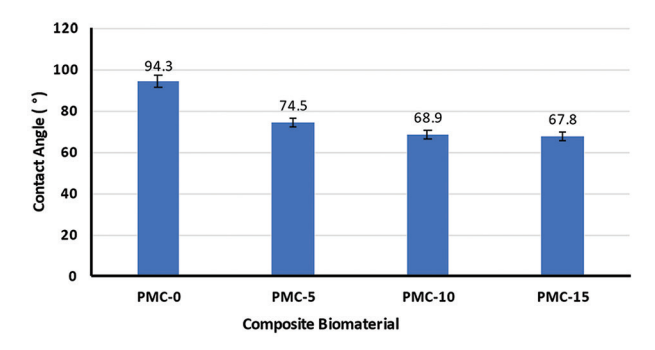


Figure 8. Water contact angle measurements of PMCs scaffolds at 90 s.

3.6. Cell viability on 3D-printed scaffolds

The biocompatibility of PMC-0 and composite scaffolds (PMC-5, PMC-10, and PMC-15) was tested by culturing NIH/3T3 cells for 3 days. Various literature has confirmed PCL's non-toxic effect on 3T3 fibroblast cells[71,72]. Hence, PCL alone was used as a control compared to other compositions. In this experiment, all the scaffolds had an average of more than 100% live cells at day 3 compared to the control one. According to the current ISO-10993, a cell viability of greater than 75% can be regarded as nontoxic for medical devices; therefore, in our experiment, we used a PCL-ceramic composition with more than 75% cell viability as a safety criterion^[73]. Tukey's post hoc test was performed with ANOVA for multiple comparisons. The α -value was set to 0.05, and P < 0.05 was considered statistically significant. No statistically significant value regarding the cellular viability of the scaffolds was observed within the groups for day 1. The cell viability of composite scaffolds was enhanced with an increase in ceramic content, as illustrated in Figure 9, using Alamar Blue assay for Day 2 and Day 3 (P < 0.05). It was demonstrated that ion-dissolution products containing Ca and Mg from bioactive glasses and ceramics enhanced cell growth [74,75]. We assume that the amount of Mg and Ca ions released from the scaffolds was not at a toxic level but instead stimulated cell proliferation.

The LDH release study also supports the viability results. Figure 9 illustrates that, after day 3, the scaffolds allowed for enhanced cell growth as the scaffolds mimicked the natural ECM for proliferation. Composite scaffolds had less toxic release than polymer-alone scaffolds (i.e., PMC-0) as the absorbance was higher due to the hydrophilicity mentioned elsewhere. Moreover, the toxicity release was lesser for PMC-5 and PMC-10. Therefore, blending CMPs with PCL improved the interaction between cells and composite scaffolds.

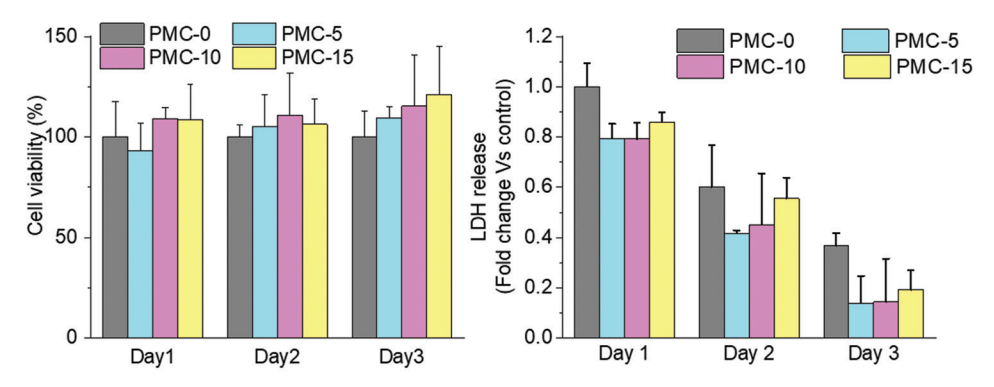


Figure 9. *In vitro* performance of 3D-printed scaffold and effects on cell viability. Left: Viability of 3T3 fibroblasts cultured on the scaffolds for 3 days (Alamar Blue assay, data normalized to values for cells cultured on control scaffolds, that is, PMC-0 [left]). Right: LDH cytotoxicity. Data represent the mean \pm S.D. (n = 3), ANOVA, *P < 0.05.

4. Conclusion

3D-printed composite scaffolds of poly(ε-caprolactone)/ calcium magnesium phosphate (PMC scaffolds) using a direct-write technique for bone tissue regeneration application were investigated. Four groups of scaffolds - PMC-0, PMC-5, PMC-10, and PMC-15 – were fabricated. The pore size of the polymer and composite scaffolds ranged between 200 and 235 µm. The polymer (PMC-0) scaffolds had a smoother surface compared to the composite scaffolds (PMC-5, PMC-10, and PMC-15). The roughness of the composite scaffold surface was due to the homogeneous dispersion of ceramic microparticles in the PCL matrix, which altered the morphology of the PCL matrix. The rheological characteristics of the composite scaffold revealed an initial Newtonian behavior but changed to a shear-thinning fluid at higher shear rates. Higher PCL-CMP blends had higher shear stress values consistent with the addition of ceramic content. The hydrophilicity of the composite scaffold improved with the incorporation of CMPs, with lower contact angles attained at higher concentrations. This can aid in the rapid proliferation and enhance the adsorption of biochemical cues for tissue regeneration. Live and death assay studies of cells indicated biocompatibility of all scaffold structures with more than 100% live cells at day 3. The cell viability of composite scaffolds was enhanced with increased ceramic content. The LDH release results illustrated that both scaffolds enhanced cell growth, mimicking the natural ECM for cell attachment and proliferation. This research lays the foundation for the bioprinting of customized composite 3D scaffold structures using custom-synthesized bioceramics for regenerative tissue engineering.

Acknowledgments

None.

Funding

The authors would like to express their gratitude for funding support from the National Science Foundation Grant (NSF CMMI Award #1663128, #2100739, #2100850) and the Center of Excellence in Product Design and Advanced Manufacturing at North Carolina A&T State University.

Conflict of interest

The authors declare no conflict of interest. The funders had no role in the design of the study; in the collection, analyses, or interpretation of data; in the writing of the manuscript, or in the decision to publish the results.

Author contributions

Conceptualization: Santosh Kumar Parupelli, Narayan Bhattarai, and Salil Desai contributed to the conceptualization of the manuscript.

Investigation: Santosh Kumar Parupelli, Sheikh Saudi conducted the investigation of the 3D Printed ceramic-PCL scaffold.

Methodology: Santosh Kumar Parupelli, and Sheikh Saudi contributed to the methodology of the research manuscript.

Resources: Narayan Bhattarai and Salil Desai provided the necessary resources for conducting the 3D printing of ceramic-PCL scaffold research work.

Writing – original draft: Santosh Kumar Parupelli, and Sheikh Saudi contributed to the writing of the original draft of the research manuscript.

Writing – review & editing: Santosh Kumar Parupelli, Narayan Bhattarai, and Salil Desai contributed to the manuscript's review and final editing.

Ethics approval and consent to participate

Not applicable.

Consent for publication

Not applicable.

Availability of data

The data presented in this study are available on request from the corresponding author.

References

- Hasan A, 2017, Tissue Engineering for Artificial Organs: Regenerative Medicine, Smart Diagnostics and Personalized Medicine. United States: John Wiley and Sons.
- 2. Van Blitterswijk C, de Boer J, Thomsen P, *et al.*, 2008, Tissue Engineering. Netherlands: Elsevier.
- 3. Williams DF, 2009, On the nature of biomaterials. *Biomaterials*, 30: 5897–5909.
 - https://doi.org/10.1016/j.biomaterials.2009.07.027
- 4. Williams DF, 2014, The biomaterials conundrum in tissue engineering. *Tissue Eng Part A*, 20: 1129–1131.
 - https://doi.org/10.1089/ten.tea.2013.0769
- 5. Lee EJ, Kasper FK, Mikos AG, 2014, Biomaterials for tissue engineering. *Ann Biomed Eng*, 42: 323–337.
 - https://doi.org/10.1007/s10439-013-0859-6
- 5. Dhandayuthapani B, Yoshida Y, Maekawa T, *et al.*, 2011, Polymeric scaffolds in tissue engineering application: A review. *Int J Polym Sci*, 2011: 290602.
 - https://doi.org/10.1155/2011/290602
- 7. Desai S, Bidanda B, Bártolo PJ, 2021, Emerging trends in

- the applications of metallic and ceramic biomaterials. In: Bio-Materials and Prototyping Applications in Medicine. Germany: Springer. p1–17.
- 8. Desai S, Shankar MR, 2021, Emerging trends in polymers, composites, and nano biomaterial applications. In: Bio-Materials and Prototyping Applications in Medicine. Germany: Springer, p19–34.
- Ratner BD, Hoffman AS, Schoen FJ, et al., 2004, Biomaterials Science: An Introduction to Materials in Medicine. San Diego, California: Academic Press. p162–164.
- 10. Hanker JS, Giammara BL, 1988, Biomaterials and biomedical devices. Science, 242: 885–892.
 - https://doi.org/10.1126/science.3055300.
- Hasirci V, Hasirci N, 2018, Fundamentals of Biomaterials. Germany: Springer.
- 12. Chen FM, Liu X, 2016, Advancing biomaterials of human origin for tissue engineering. *Prog Polym Sci*, 53: 86–168.

https://doi.org/10.1016/j.progpolymsci.2015.02.004

13. O'Brien FJ, 2011, Biomaterials and scaffolds for tissue engineering. *Mater Today*, 14: 88–95.

https://doi.org/10.1016/S1369-7021(11)70058-X

- Keane TJ, Badylak SF, 2014, Biomaterials for tissue engineering applications. In: Seminars in Pediatric Surgery. Vol. 23. Netherlands: Elsevier. p112–118.
- 15. Burdick JA, Mauck RL, 2010, Biomaterials for Tissue Engineering Applications: A Review of the Past and Future Trends. Germany: Springer.
- 16. López-Rodríguez N, López-Arraiza A, Meaurio E, *et al.*, 2006, Crystallization, morphology, and mechanical behavior of polylactide/poly (ε-caprolactone) blends. *Polym Eng Sci*, 46: 1299–1308.

https://doi.org/10.1002/pen.20609

17. Yoshimoto H, Shin YM, Terai H, *et al.*, 2003, A biodegradable nanofiber scaffold by electrospinning and its potential for bone tissue engineering. *Biomaterials*, 24: 2077–2082.

https://doi.org/10.1016/s0142-9612(02)00635-x

18. Rezwan K, Chen QZ, Blaker JJ, *et al.*, 2006, Biodegradable and bioactive porous polymer/inorganic composite scaffolds for bone tissue engineering. *Biomaterials*, 27: 3413–3431.

https://doi.org/10.1016/j.biomaterials.2006.01.039

19. Ma PX, 2004, Scaffolds for tissue fabrication. *Mater Today*, 7: 30–40.

https://doi.org/10.1016/S1369-7021(04)00233-0

20. Choi SW, Zhang Y, Xia Y, 2010, Three-dimensional scaffolds for tissue engineering: The importance of uniformity in pore size and structure. *Langmuir*, 26: 19001–19006.

https://doi.org/10.1021/la104206h

- 21. Desai S, Harrison B, 2010, Direct-writing of biomedia for drug delivery and tissue regeneration. In: Printed Biomaterials: Novel Processing and Modeling Techniques for Medicine and Surgery. Germany: Springer Verlag.
- Desai S, Perkins J, Harrison BS, et al., 2010, Understanding release kinetics of biopolymer drug delivery microcapsules for biomedical applications. Mater Sci Eng B, 168: 127–131.

https://doi.org/10.1016/j.mseb.2009.11.006

- 23. Desai S, Moore A, Harrison B, *et al.*, 2008, Understanding microdroplet formations for biomedical applications. In: ASME International Mechanical Engineering Congress and Exposition. New York, United States: ASME. p1–4.
- Abedalwafa M, Wang F, Wang L, et al., 2013, Biodegradable poly-epsilon-caprolactone (PCL) for tissue engineering applications: A review. Rev Adv Mater Sci, 34: 123–140.
- 25. Grandi C, di Liddo R, Paganin P, et al., 2011, Porous alginate/poly (ε-caprolactone) scaffolds: Preparation, characterization and *in vitro* biological activity. *Int J Mol Med*, 27: 455–467.

https://doi.org/10.3892/ijmm.2010.593

- Zhang XC, 2016, Science and Principles of Biodegradable and Bioresorbable Medical Polymers: Materials and Properties. Sawston, United Kingdom: Woodhead Publishing.
- 27. Li W, Danielson KG, Alexander PG, *et al.*, 2003, Biological response of chondrocytes cultured in three-dimensional nanofibrous poly (ε-caprolactone) scaffolds. *J Biomed Mater Res A*, 67: 1105–1114.

https://doi.org/10.1002/jbm.a.10101

28. Albertsson AC, Varma IK, 2003, Recent developments in ring opening polymerization of lactones for biomedical applications. *Biomacromolecules*, 4: 1466–1486.

https://doi.org/10.1021/bm034247a

29. Saudi S, Bhattarai SR, Adhikari U, *et al.*, 2020, Nanonetnano fiber electrospun mesh of PCL-chitosan for controlled and extended release of diclofenac sodium. *Nanoscale*, 12: 23556–23569.

https://doi.org/10.1039/D0NR05968D

30. Adarkwa E, Kotoka R, Desai S, 2021, 3D printing of polymeric Coatings on AZ31 Mg alloy Substrate for Corrosion Protection of biomedical implants. *Med Devices Sens*, 4: e10167.

https://doi.org/10.1002/MDS3.10167

 Marquetti I, Desai S, 2018, Adsorption behavior of bone morphogenetic protein-2 on a graphite substrate for biomedical applications. Am J Eng Appl Sci, 11: 1037–1044.

https://doi.org/10.3844/ajeassp.2018.1037.1044

32. Wu F, Liu C, O'Neill B, *et al.*, 2012, Fabrication and properties of porous scaffold of magnesium phosphate/ polycaprolactone biocomposite for bone tissue engineering.

Appl Surf Sci, 258: 7589-7595.

https://doi.org/10.1016/j.apsusc.2012.04.094

33. Liu L, Wang Y, Guo S, *et al.*, 2012, Porous polycaprolactone/ nanohydroxyapatite tissue engineering scaffolds fabricated by combining NaCl and PEG as co-porogens: Structure, property, and chondrocyte-scaffold interaction *in vitro*. *J Biomed Mater Res B Appl Biomater*, 100: 956–966.

https://doi.org/10.1002/JBM.B.32658

34. Diba M, Kharaziha M, Fathi MH, *et al.*, 2012, Preparation and characterization of polycaprolactone/forsterite nanocomposite porous scaffolds designed for bone tissue regeneration. *Compos Sci Technol*, 72: 716–723.

https://doi.org/10.1016/J.COMPSCITECH.2012.01.023

35. Lei B, Shin KH, Noh DY, *et al.*, 2012, Bioactive glass microspheres as reinforcement for improving the mechanical properties and biological performance of poly(ε-caprolactone) polymer for bone tissue regeneration. *J Biomed Mater Res B Appl Biomater*, 100B: 967–975.

https://doi.org/10.1002/JBM.B.32659

 Dong Z, Wu Y, Wang Q, et al., 2012, Reinforcement of electrospun membranes using nanoscale Al2O3 whiskers for improved tissue scaffolds. J Biomed Mater Res A, 100: 903–910.

https://doi.org/10.1002/jbm.a.34027

37. Marquetti I, Desai S, 2019, Orientation effects on the nanoscale adsorption behavior of bone morphogenetic protein-2 on hydrophilic silicon dioxide. *RSC Adv*, 9: 906–916.

https://doi.org/10.1039/C8RA09165J

 Marquetti I, Desai S, 2018, Molecular modeling the adsorption behavior of bone morphogenetic protein-2 on hydrophobic and hydrophilic substrates. *Chem Phys Lett*, 706: 285–294.

https://doi.org/10.1016/j.cplett.2018.06.015

39. Marquetti I, Desai S, 2022, An atomistic investigation of adsorption of bone morphogenetic protein-2 on gold with nanoscale topographies. *Surfaces*, 5: 176–185.

https://doi.org/10.3390/surfaces5010010

40. Huang B, Caetano G, Vyas C, *et al.*, 2018, Polymer-ceramic composite scaffolds: The effect of hydroxyapatite and β -tricalcium phosphate. *Materials*, 11: 129.

https://doi.org/10.3390/ma11010129

41. Klein CP, Driessen AA, de Groot K, *et al.*, 1983, Biodegradation behavior of various calcium phosphate materials in bone tissue. *J Biomed Mater Res*, 17: 769–784.

https://doi.org/10.1002/jbm.820170505

42. Parupelli S, Desai S, 2019, A comprehensive review of additive manufacturing (3d printing): Processes, applications and future potential. *Am J Appl Sci*, 16: 244–272.

https://doi.org/10.3844/ajassp.2019.244.272

- 43. Parupelli SK, Aljohani A, Desai S, 2019, Direct jet printing and characterization of calcium alginate microcapsules for biomedical applications. In: Proceedings of the 2019 IISE Annual Conference. Florida, USA: Institute of Industrial and Systems Engineers (IISE).
- 44. Perkins J, Xu Z, Smith C, *et al.*, 2015, Direct writing of polymeric coatings on magnesium alloy for tracheal stent applications. *Ann Biomed Eng*, 43: 1158–1165.

https://doi.org/10.1007/s10439-014-1169-3

Papaioannou TG, Manolesou D, Dimakakos E, et al., 2019,
 Bioprinting methods and techniques: Applications on artificial blood vessel fabrication. Acta Cardiol Sin, 35: 284.

https://doi.org/10.6515/ACS.201905_35(3).20181115A

46. Ning L, Chen X, 2017, A brief review of extrusion-based tissue scaffold bio-printing. *Biotechnol J*, 12: 1600671.

https://doi.org/10.1002/BIOT.201600671

47. Deo KA, Singh KA, Peak CW, et al., 2020, Bioprinting 101: Design, fabrication, and evaluation of cell-laden 3D bioprinted scaffolds. *Tissue Eng Part A*, 26: 318–338.

https://doi.org/10.1089/TEN.TEA.2019.0298

48. Kačarević ŽP, Rider PM, Alkildani S, *et al.*, 2018, An introduction to 3D bioprinting: Possibilities, challenges and future aspects. *Materials*, 11: 2199.

https://doi.org/10.3390/MA11112199

49. Agarwal S, Saha S, Balla VK, *et al.*, 2020, Current developments in 3D bioprinting for tissue and organ regeneration-a review. *Front Mech Eng*, 6: 589171.

https://doi.org/10.3389/FMECH.2020.589171

 Gmeiner R, Deisinger U, Schönherr J, et al., 2015, Additive manufacturing of bioactive glasses and silicate bioceramics. I Ceram Sci. 6: 75–86.

https://doi.org/10.4416/JCST2015-00001

51. Sobral JM, Caridade SG, Sousa RA, et al., 2011, Three-dimensional plotted scaffolds with controlled pore size gradients: Effect of scaffold geometry on mechanical performance and cell seeding efficiency. Acta Biomater, 7: 1009–1018.

https://doi.org/10.1016/j.actbio.2010.11.003

52. Chen WH, Liu YY, Zhang FH, *et al.*, 2015, Osteochondral integrated scaffolds with gradient structure by 3D printing forming. *Int J Autom Comput*, 12: 220–228.

https://doi.org/10.1007/s11633-014-0853-y

53. Thomas M, Willerth SM, 2017, 3-D bioprinting of neural tissue for applications in cell therapy and drug screening. *Front Bioeng Biotechnol*, 5: 69.

https://doi.org/10.3389/fbioe.2017.00069

54. Kundu J, Shim JH, Jang J, et al., 2015, An additive manufacturing-based PCL-alginate-chondrocyte bioprinted

scaffold for cartilage tissue engineering. J Tissue Eng Regen Med, 9: 1286–1297.

https://doi.org/10.1002/term.1682

55. Ma J, Lin L, Zuo Y, *et al.*, 2019, Modification of 3D printed PCL scaffolds by PVAc and HA to enhance cytocompatibility and osteogenesis. *RSC Adv*, 9: 5338–5346.

https://doi.org/10.1039/C8RA06652C

56. Adhikari U, Rijal NP, Khanal S, et al., 2016, Magnesium and calcium-containing scaffolds for bone tissue regeneration. In: ASME International Mechanical Engineering Congress and Exposition. Vol. 50688. New York, United States: American Society of Mechanical Engineers.

https://doi.org/10.1115/IMECE2016-66835

57. Schneider CA, Rasband WS, Eliceiri KW, 2012, NIH Image to ImageJ: 25 years of image analysis. *Nat Methods*, 9: 671–675.

https://doi.org/10.1038/nmeth.2089

58. Huang B, Bártolo PJ, 2018, Rheological characterization of polymer/ceramic blends for 3D printing of bone scaffolds. *Polym Test*, 68: 365–378.

https://doi.org/10.1016/j.polymertesting.2018.04.033

59. Jiang W, Shi J, Li W, et al., 2012, Morphology, wettability, and mechanical properties of polycaprolactone/hydroxyapatite composite scaffolds with interconnected pore structures fabricated by a mini-deposition system. *Polym Eng Sci*, 52: 2396–2402.

https://doi.org/10.1002/pen.23193

60. Jia J, Zhou H, Wei J, *et al.*, 2010, Development of magnesium calcium phosphate biocement for bone regeneration. *J R Soc Interface*, 7: 1171–1180.

https://doi.org/10.1098/rsif.2009.0559

61. Fazeli N, Arefian E, Irani S, *et al.*, 2021, 3D-printed PCL scaffolds coated with nanobioceramics enhance osteogenic differentiation of stem cells. *ACS Omega*, 6: 35284–35296.

https://doi.org/10.1021/acsomega.1c04015

62. Yang X, Wang Y, Zhou Y, *et al.*, 2021, The application of polycaprolactone in three-dimensional printing scaffolds for bone tissue engineering. *Polymers (Basel)*, 13: 2754.

https://doi.org/10.3390/polym13162754

63. Liu D, Nie W, Li D, *et al.*, 2019, 3D printed PCL/SrHA scaffold for enhanced bone regeneration. *Chem Eng J*, 362: 269–279.

https://doi.org/10.1016/j.cej.2019.01.015

64. Park SA, Lee SJ, Seok JM, *et al.*, 2018, Fabrication of 3D printed PCL/PEG polyblend scaffold using rapid prototyping system for bone tissue engineering application. *J Bionic Eng*, 15: 435–442.

https://doi.org/10.1007/s42235-018-0034-8

65. Park SA, Lee HJ, Kim KS, *et al.*, 2018, *In vivo* evaluation of 3D-printed polycaprolactone scaffold implantation combined with β-TCP powder for alveolar bone augmentation in a beagle defect model. *Materials*, 11: 238.

https://doi.org/10.3390/ma11020238

66. Murphy CM, Haugh MG, O'brien FJ, 2010, The effect of mean pore size on cell attachment, proliferation and migration in collagen-glycosaminoglycan scaffolds for bone tissue engineering. *Biomaterials*, 31: 461–466.

https://doi.org/10.1016/j.biomaterials.2009.09.063

67. O'Brien FJ, Harley BA, Yannas IV, et al., 2005, The effect of pore size on cell adhesion in collagen-GAG scaffolds. *Biomaterials*, 26: 433–441.

https://doi.org/10.1016/j.biomaterials.2004.02.052

68. Wibowo A, Vyas C, Cooper G, *et al.*, 2020, 3D printing of polycaprolactone-polyaniline electroactive scaffolds for bone tissue engineering. *Materials*, 13: 512.

https://doi.org/10.3390/ma13030512

69. Loh QL, Choong C, 2013, Three-dimensional scaffolds for tissue engineering applications: Role of porosity and pore size. Tissue Eng Part B Rev, 19: 485–502.

https://doi.org/10.1089/ten.TEB.2012.0437

70. Karageorgiou V, Kaplan D, 2005, Porosity of 3D biomaterial scaffolds and osteogenesis. *Biomaterials*, 26: 5474–5491.

https://doi.org/10.1016/j.biomaterials.2005.02.002

71. Edwards A, Jarvis D, Hopkins T, *et al.*, 2015, Poly (ε-caprolactone)/keratin-based composite nanofibers for biomedical applications. *J Biomed Mater Res B Appl Biomater*, 103: 21–30.

https://doi.org/10.1002/jbm.b.33172

72. Gomes SR, Rodrigues G, Martins GG, *et al.*, 2015, *In vitro* and *in vivo* evaluation of electrospun nanofibers of PCL, chitosan and gelatin: A comparative study. *Mater Sci Eng C*, 46: 348–358.

https://doi.org/10.1016/j.msec.2014.10.051

73. Wang J, Witte F, Xi T, *et al.*, 2015, Recommendation for modifying current cytotoxicity testing standards for biodegradable magnesium-based materials. *Acta Biomater*, 21: 237–249.

https://doi.org/10.1016/j.actbio.2015.04.011

 Dietrich E, Oudadesse H, Lucas-Girot A, et al., 2009, *In vitro* bioactivity of melt-derived glass 46S6 doped with magnesium. *J Biomed Mater Res A*, 88: 1087–1096.

https://doi.org/10.1002/jbm.a.31901

75. Sader MS, LeGeros RZ, Soares GA, 2009, Human osteoblasts adhesion and proliferation on magnesium-substituted tricalcium phosphate dense tablets. *J Mater Sci Mater Med*, 20: 521–527.

https://doi.org/10.1007/s10856-008-3610-3